北見工業大学研究報告
第12巻 第2号 (昭和56年)

Memoirs of the Kitami Institute of Technology
Vol. 12 No. 2 (1981)

A Flow around a Hemisphere Mounted on a Plane Wall

by Seiichi TANIGUCHI*, Katumi MIYAKOSHI*
Toshiharu IKEDA**
and Kazuya NAKAMURA***

(Received September 10, 1980)

Abstract

Time-averaged pressure distributions on the surface of a hemisphere immersed in a fully-developed turbulent boundary layer on a smooth plane wall were measured in order to elucidate the relation between aerodynamic force acting on the hemisphere and characteristics of the boundary layers. The drag coefficient defined by $C_{D\tau}=D\Big/\left(\frac{1}{2}\rho u_\tau^2 A\right)$ was found to be expressed by a power function solely of du_τ/ν in the region $d/\delta\lesssim 1.0$, where D is the form drag, u_τ the shear velocity, ν the kinematic viscosity and A the projectional area of the hemisphere, respectively.

1. Introduction

The flow around a three-dimensional bluff body mounted on a plane wall reveals some interesting and complicated phenomena. Namely, the boundary layer upstream of a bluff body encounters an adverse pressure gradient, so that a three-dimensional separation is induced at a certain distance upstream of the obstacle. The separated flow rolls itself up downstream and surrounds the bluff body to form a system of horse shoe vortices. Further, the flow separeted on the obstacle wraps up and becomes a so-called arch-typed vortex.

In engineering, the aerodynamic behaviour of a three-dimensional bluff body immersed in a turbulent boundary layer has attracted the attention of many investigators in the field of industrial aerodynamics. Okamoto [1] and Fiedler [2] have studied fluid force and wake formation of right circular cylinders of finite height. Castro and Robins [3] and Okamoto [4] have investigated aerodynamic characteristics of cube and cone, respectively. There exist many practical problems relating to this category of flow, but theoretical treatment is almost impossible, except for a few cases of numerical investigation of the laminar condition (Mason and Sykes [5], Daiguji [6]). This is because of their complicated nature and the lack of knowledge about such flows.

In previous papers (Taniguchi [7], Sakamoto [8]), the relation between the aerodynamic forces of right circular cylinders and cubes, cited as typical three-dimensional bluff bodies, and the characteristics of the boundary layer flows

* Department of Applied Mechanical Engineering, Kitami Institute of Technology.
** Asahikawa Nissan Automobile Co. Ltd.
*** Showa Seiki Co. Ltd.

were investigated. It was found in these papers that there existed a power functional relationship between the drag coefficient C_D and h/δ (h is the height of the bluff body and δ is the thickness of the boundary layer). Further, it was established that the parameters included in the power functions varied according to the geometrical shape of the bluff body. Consequently, characteristics of the flows around each bluff body must be investigated separately because the parameters included in the power function have not a generalized relationship for bluff body.

The present study describes the time-averaged aerodynamic behaviour of the hemisphere cited another typical three-dimensional bluff body. This, too, was mounted on a plane wall and then a turbulent boundary layer fully developed. The flow around a hemisphere is of great importance in evaluating the effect of tides and waves upon underwater construction and that of wind gusts on captive balloons. It is also important to understand more about the performance of vortex generator of the hemisphere. A few experimental studies on the flow around a hemisphere (Jacobs [9], Wieghart [10] and Wooding [11]) have been undertaken. However, a systematic investigation clarifying the relationship between variation of the geometrical size of the hemisphere and the characteristics of the boundary layer has not been performed yet. Accordingly, engineers of industrial aerodynamics and architectonics will find the present data useful.

2. Experimental apparatus and procedures

The experiment was carried out in a wind tunnel of low-speed and closed-return type with a test section 0.4 m high, 0.4 m wide and about 4 m long. A series of three turbulence-reducing screens was installed in the calming chamber upstream of the contraction channel (contraction ratio 14 : 1). The ceiling of the test section was made of a flexible sheet with eighteen pressure taps of 0.5 mm diameter, so that its shape could be adjusted to change the longitudinal pressure gradient. The floor of the test section was made of smooth plates of acrylic resin and a steel plate 460 mm long on which a hemisphere was mounted.

The hemisphere was set up on the supporting equipment 23.55 cm downstream from the entrance of the test section as shown in Fig. 1. In the present experiment, the diameters of hemisphere selected for pressure measurement were 10, 15, 20, 25, 30, 40, 50, 60 and 70 mm. Each body was almost totally immersed in the turbulent boundary layer except for a few of the large ones. The hemispheres were made of brass and a considerable number of 0.4～0.5 mm piezometric were drilled on their surfaces. These piezometric holes were arranged in a longitudinal line on the hemisphere at a distance 6°～10°. The body could be rotated about its axis so that the pressure distribution on the whole surface of the hemisphere could be measured using these piezometric holes. Figure 2 shows a definition sketch of a test hemisphere and the coordinate system used in the present experiment.

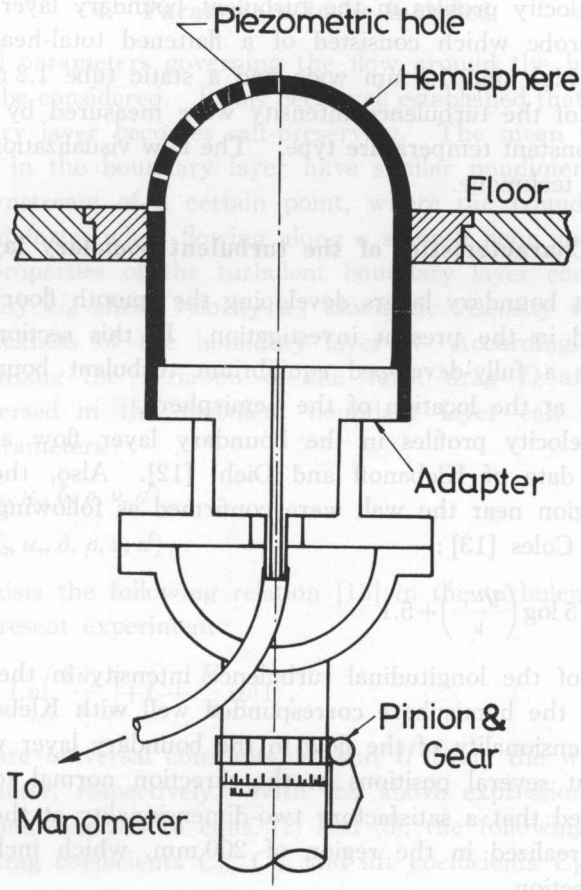

Fig. 1. Cross section of a hemisphere.

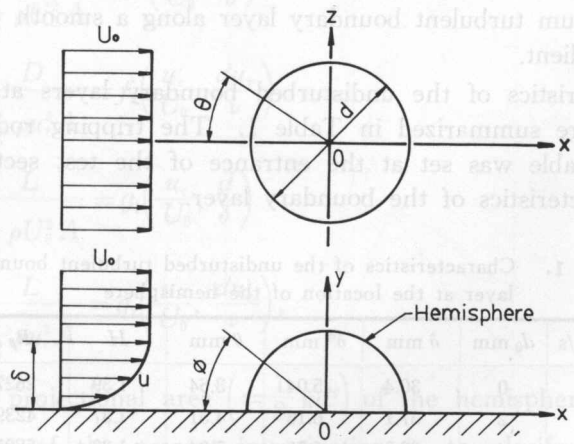

Fig. 2. Coordinate system and definition sketch.

The mean velocity profiles in the turbulent boundary layer were measured by means of a probe which consisted of a flattened total-head tube with an opening 0.44 mm high and 1.8 mm wide and a static tube 1.2 mm in diameter. The distributions of the turbulence intensity were measured by a hot-wire anemometer of the constant temperature type. The flow visualization was performed using the oil film technique.

3. Characteristics of the turbulent boundary layer

The turbulent boundary layers developing the smooth floor of the test section were adopted in the present investigation. In this section, it will be ascertained whether a fully-developed equilibrium turbulent boundary layer was estabilshed or not at the location of the hemisphere.

The mean velocity profiles in the boundary layer flow agreed well with the experimental data of Klebanoff and Diehl [12]. Also, the mean velocity profiles in the region near the wall were confirmed as following the logarithmic law suggested by Coles [13]:

$$\frac{u}{u_\tau}=5.75\log\left(\frac{yu_\tau}{\nu}\right)+5.1 \qquad (1)$$

The distribution of the longitudinal turbulence intensity in the boundary layer at the location of the hemisphere corresponded well with Klebanoff's data [12].

The two-dimensionality of the flow in the boundary layer was examined by velocity profiles at several positions in the direction normal to a free stream. The results showed that a satisfactory two-dimensionality at the location of the hemisphere was realized in the region of 200 mm, which included the center line of the test section.

From the above, it could be concluded that the turbulent boundary layer employed in the present investigation had the same characteristics as a fully-developed equilibrium turbulent boundary layer along a smooth plane wall under zero pressure gradient.

The characteristics of the undisturbed boundary layers at the location of the hemisphere are summarized in Table 1. The tripping rod of diameter d_0 included in this table was set at the entrance of the test section in order to change the characteristics of the boundary layer.

Table 1. Characteristics of the undisturbed turbulent boundary layer at the location of the hemisphere

RUN	U_0 m/s	d_0 mm	δ mm	δ^* mm	θ mm	H	R_θ	u_τ/U_0
1	12	0	30.4	5.04	3.64	1.39	2627	0.0408
2	16	2	37.1	6.16	4.51	1.37	4239	0.0390
3	20	4	46.9	6.70	5.04	1.33	5805	0.0379
4	16	0	29.6	4.72	3.45	1.37	3285	0.0401
5	20	2	35.7	5.58	4.14	1.35	4915	0.0385

4. Parameters to be included

The physical parameters governing the flow around the hemisphere set on a plane wall first be considered. It has been well established that a fully-developed turbulent boundary layer becomes self-preserving. The mean velocity and turbulent properties in the boundary layer have similar nondimensional profiles at each station downstream of a certain point, where the boundary layer attains its fully developed form, when flowing along a smooth floor under zero pressure gradient. The properties of the turbulent boundary layer can be specified by free-stream velocity U_0, shear velocity u_τ, kinematic viscosity ν, density of the fluid ρ and thickness of the boundary layer δ. Accordingly, the functional relationship describing the variation of the form drag D and lift L of the hemisphere immersed in the turbulent boundary layer can be expressed by these physical parameters:

$$D=f(U_0, u_\tau, \delta, \rho, \nu, d) \tag{2}$$

$$L=g(U_0, u_\tau, \delta, \rho, \nu, d)\,. \tag{3}$$

Further, there exists the following relation [13] in the turbulent boundary layer adopted in the present experiment:

$$\frac{u}{u_\tau}=\frac{1}{\kappa}Ln\left(\frac{\delta u_\tau}{\nu}\right)+C+\frac{\Pi}{\kappa}w(1)\,, \tag{4}$$

where κ and C are universal constants, w and Π being the wake function and the profile parameter, respectively. With the above expression in mind, when applying dimensional analysis to eqns. (2) and (3), the following functional relationships about drag coefficients C_D, C_{D_τ} and lift coefficients C_L, C_{L_τ} can be induced:

$$C_D=\frac{D}{\frac{1}{2}\rho U_0^2 A}=f_1\left(\frac{u_\tau}{U_0}, \frac{d}{\delta}\right) \tag{5}$$

$$C_{D_\tau}=\frac{D}{\frac{1}{2}\rho u_\tau^2 A}=f_2\left(\frac{u_\tau}{U_0}, \frac{du_\tau}{\nu}\right) \tag{6}$$

$$C_L=\frac{L}{\frac{1}{2}\rho U_0^2 A}=g_1\left(\frac{u_\tau}{U_0}, \frac{d}{\delta}\right) \tag{7}$$

$$C_{L_\tau}=\frac{L}{\frac{1}{2}\rho u_\tau^2 A}=g_2\left(\frac{u_\tau}{U_0}, \frac{du_\tau}{\nu}\right), \tag{8}$$

where A is the projectional area $\left(=\frac{1}{8}\pi d^2\right)$ of the hemisphere. Consequently, the main purpose of the present investigation is to clarify these functional relationships of eqn. (5)~(8) varying the above sets of two nondimensional parameters.

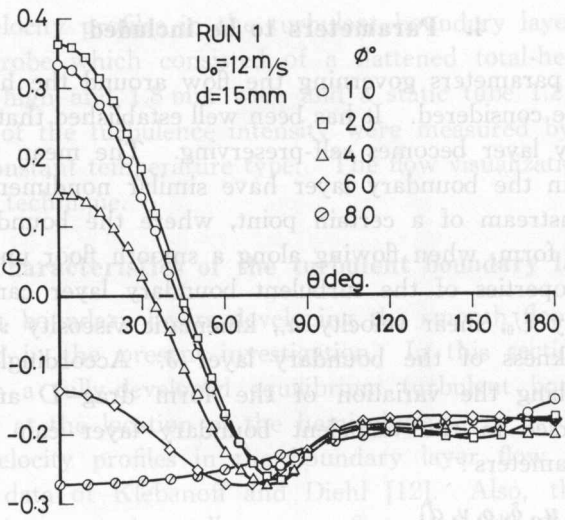

(a)

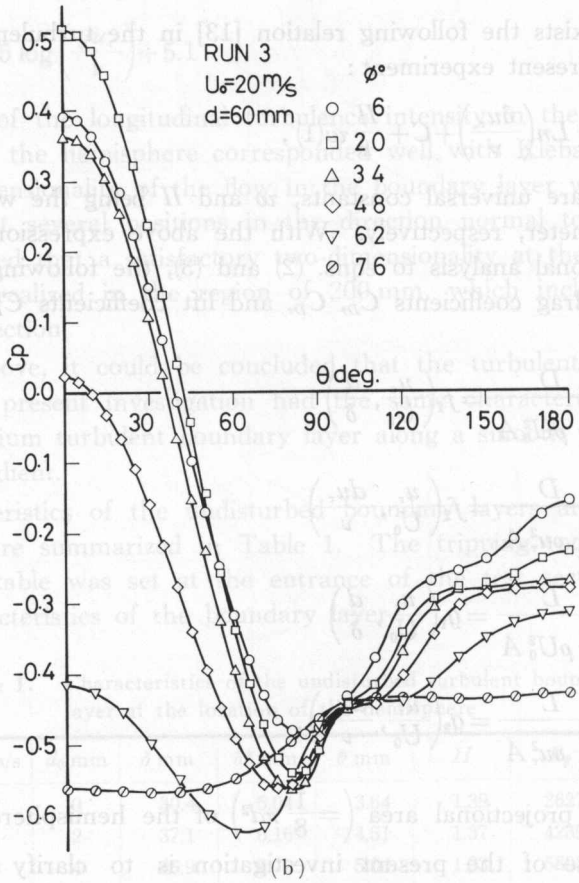

(b)

Fig. 3. Pressure distributions on hemispheres
(a) $d=15$ mm, $U_0=12$ m/s, (b) $d=60$ mm, $U_0=20$ m/s.

5. Pressure distributions on and around the hemisphere

A few examples of the pressure distributions on the surface of a hemisphere are shown in the form of the pressure coefficient c_p versus angle θ in Fig. 3 (a), (b). The pressure coefficient has been defined as

$$c_p = (p - p_0) \Big/ \left(\frac{1}{2} \rho U_0^2 \right),$$

where p is the presure on the surface of the hemisphere and p_0 is the static pressure of the free stream. The profiles of the pressure distributions are similar to those of the right circular cylinder [7] in the range of the smaller angle ϕ. However, all the values of pressure on the surface drop under the static pressure

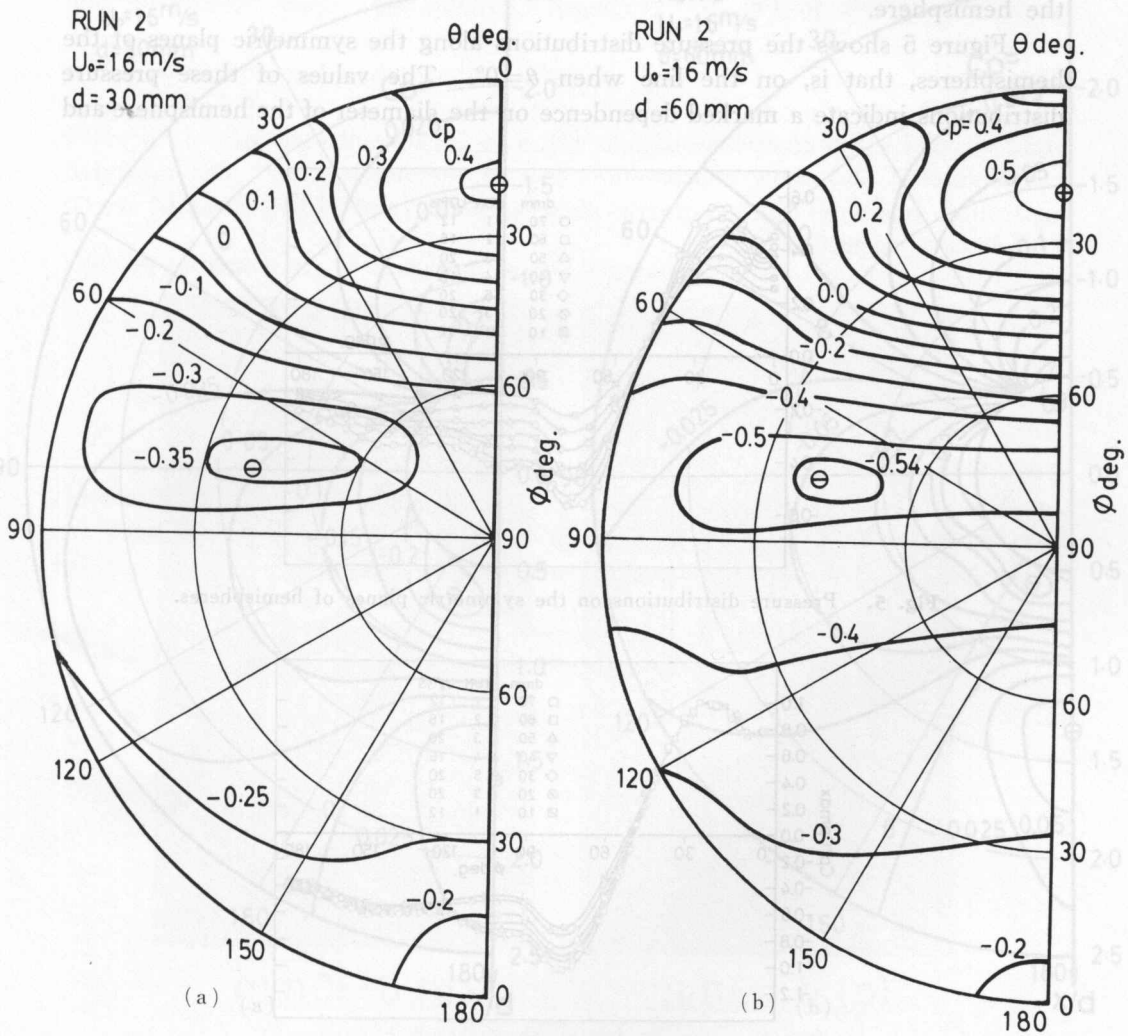

Fig. 4. Iso-pressure line on hemispheres.
(a) $d=30$ mm, $U_0=16$ m/s, (b) $d=60$ mm, $U_0=16$ m/s.

of the free stream when $\phi \gtrsim 50°$. Further, the back pressure of the smaller hemisphere $d=30$ mm has an almost constant value irrespective of the variation of ϕ. In contrast, the difference in the back pressure attains a considerably greater magnitude in the case of the larger hemisphere $d=60$ mm.

Figure 4 shows the pressure distributions with iso-pressure lines also in the form of the pressure coefficient c_p. As will be seen in this figure, the maximum and minimum values of the pressure on the surface of the hemisphere are found at the locations of $\theta \cong 0°$, $\phi \cong 20°$ and $\theta \cong 75°$, $\phi \cong 40°$, respectively. It was confirmed that these locations scarcely moved despite variations in the size of the hemisphere and the characteristics of the boundary layer under the present experimental conditions. It may be noted in these figures that the iso-pressure lines almost parallel to the z-axis except for the upstream part of the surface of the hemisphere.

Figure 5 shows the pressure distributions along the symmetric planes of the hemispheres, that is, on the line when $\theta=0°$. The values of these pressure distributions indicate a marked dependence on the diameter of the hemisphere and

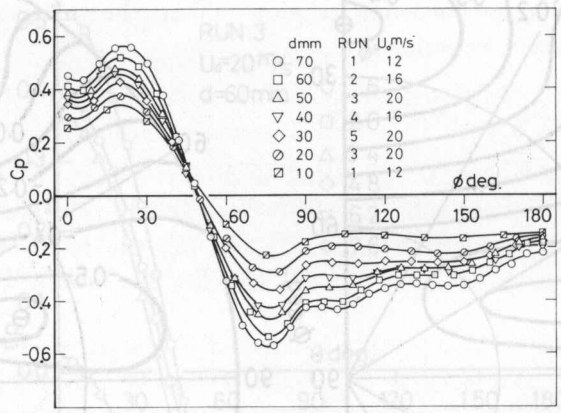

Fig. 5. Pressure distributions on the symmetric planes of hemispheres.

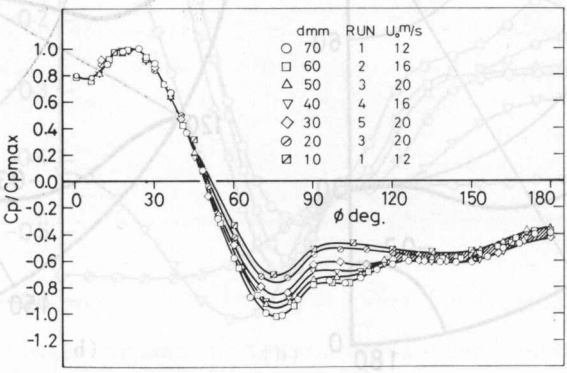

Fig. 6. Similarity of the pressure distributions on the symmetric planes of hemispheres.

the velocity of the flow, namely, Reynolds number ($U_0 d/\nu$). The differences of pressure in the range $50° \leq \phi \leq 180°$ might be considered to be number. due to the fact that the wake flow pattern was changed by variation of Reynolds However, the increment of pressure on the front surface of the hemisphere may be based on the fact that the pressure on the larger hemisphere must be more strongly influenced by the relatively higher velocity of the boundary flow, so that the amount of pressure on the front surface of the hemisphere increases.

Next, similality of the pressure distributions on the surfaces of the hemisphere will be tested. Figure 6 represents the pressure distribution on the sym-

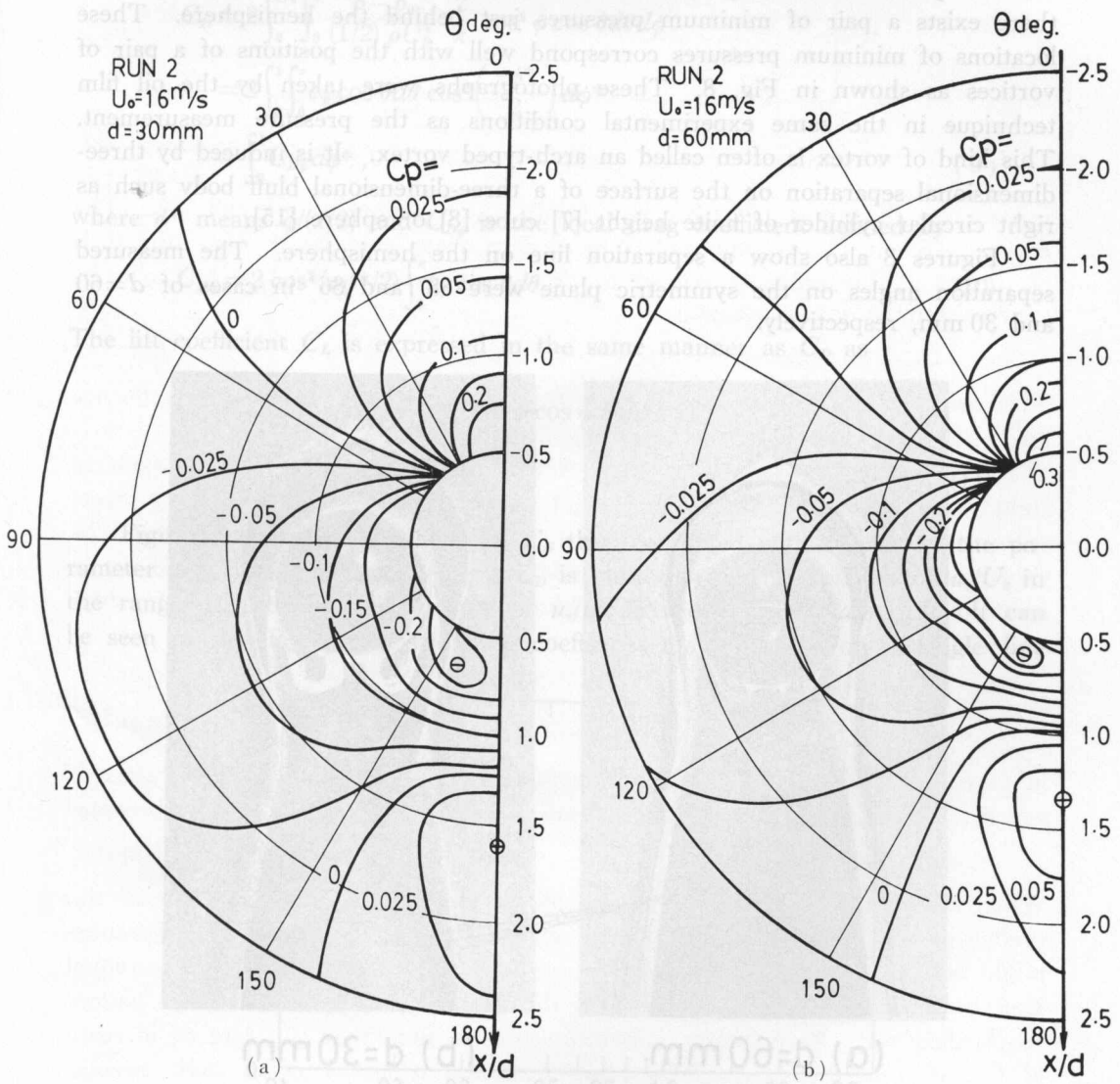

Fig. 7. Iso-pressure line on the plane wall around a hemisphere.
(a) $d=30$ mm, $U_0=16$ m/s, (b) $d=60$ mm, $U_0=16$ m/s.

metric plane of the hemisphere in the form of $c_p/c_{p\max}$ versus ϕ, where $c_{p\max}$ is the maximum value of the pressure coefficient described just above. These pressure profiles exhibit a high degree of similality in the range $0° \leq \phi \leq 50°$ and $120° \leq \phi \leq 180°$, respectively. However, there are considerable differences of $c_p/c_{p\max}$ in the range $50° \leq \phi \leq 120°$. This might occur because of changes in the flow pattern on the hemisphere with variation of the Reynolds number, as has been explained above.

Figures 7 (a), (b) represent pressure distributions, with the iso-pressure line in the form of c_p, on the plane wall around the hemisphere. It will be noted that the pressure on the plane wall is positive in the range $0° \leq \phi \leq 50°$. Also, there exists a pair of minimum pressures just behind the hemisphere. These locations of minimum pressures correspond well with the positions of a pair of vortices as shown in Fig. 8. These photographs were taken by the oil film technique in the same experimental conditions as the pressure measurement. This kind of vortex is often called an arch-typed vortex. It is induced by three-dimensional separation on the surface of a three-dimensional bluff body such as right circular cylinder of finite height [7] cube [8] or sphere [15].

Figures 8 also show a separation line on the hemisphere. The measured separation angles on the symmetric plane were 88° and 86° in cases of $d=60$ and 30 mm, respectively.

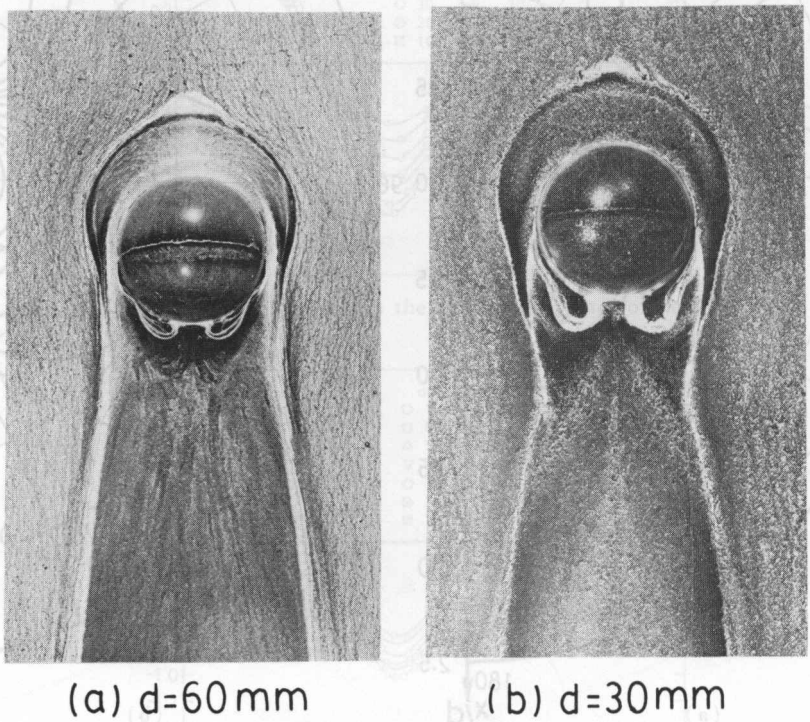

Fig. 8. Visualization of the surface flow patterns.
(a) $d=30$ mm, $U_0=16$ m/s, (b) $d=60$ mm, $U_0=16$ m/s.

6. Fluid forces on a hemisphere

There are two fluid forces on a hemisphere. One is the pressure force due to pressure difference and the other is the viscous force due to the shear stress acting on the surface of the hemisphere. However, in this investigation, attention will be paid only to the pressure force, because its order of magnitude is much larger than the viscous shear force.

Since the flow around the hemisphere is symmetric about the x-axis, the drag coefficient C_D based on the pressure difference is integrated as

$$\begin{aligned} C_D &= 2\int_0^{\pi/2}\int_0^{\pi} \frac{p-p_0}{(1/2)\,\rho U_0^2}\,\frac{2}{\pi}\cos^2\phi\cos\theta\, d\theta d\phi \\ &= 2\int_0^1\int_0^{\pi} c_p\cos\theta\, d\theta\cos^2\left(\frac{\pi\phi^*}{2}\right)d\phi^* \\ &= \int_0^1 C_{D\phi}\, d\phi^*, \end{aligned} \tag{9}$$

where ϕ^* means $\phi/(\pi/2)$ and $C_{D\phi}$ is the local drag coefficient defined by

$$C_{D\phi} = 2\cos^2(\pi\phi^*/2)\int_0^{\pi} c_p\cos\theta\, d\theta \tag{10}$$

The lift coefficient C_L is expressed in the same manner as C_D as

$$\begin{aligned} C_L &= 2\int_0^{\pi/2}\int_0^{\pi} \frac{p-p_0}{(1/2)\,\rho U_0^2}\,\frac{2}{\pi}\sin\phi\cos\phi\, d\theta d\phi \\ &= \int_0^1\int_0^{\pi} c_p\sin(\pi\phi^*)\, d\theta d\phi\,. \end{aligned} \tag{11}$$

Figure 9 shows the variation of C_D thus computed with respect to the parameter d/δ. On this log-log sheet, C_D is plotted with three values of u_τ/U_0 in the range $d/\delta \leq 1.0$ and five values of u_τ/U_0 in the range of $d/\delta \geq 1.0$. It can be seen in this figure that the drag coefficient C_D is plotted on a single line

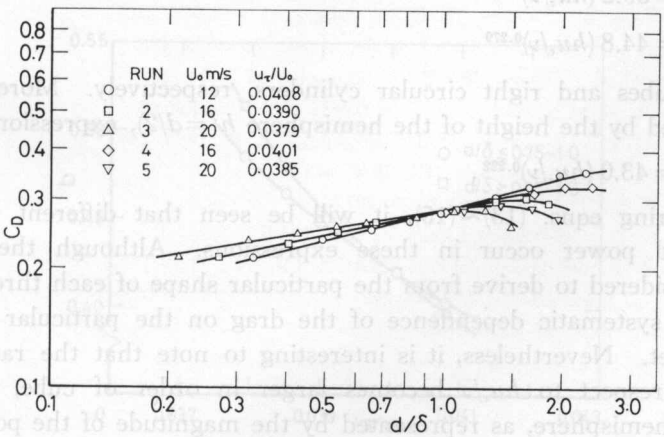

Fig. 9. Relation between drag coefficient C_D and d/δ.

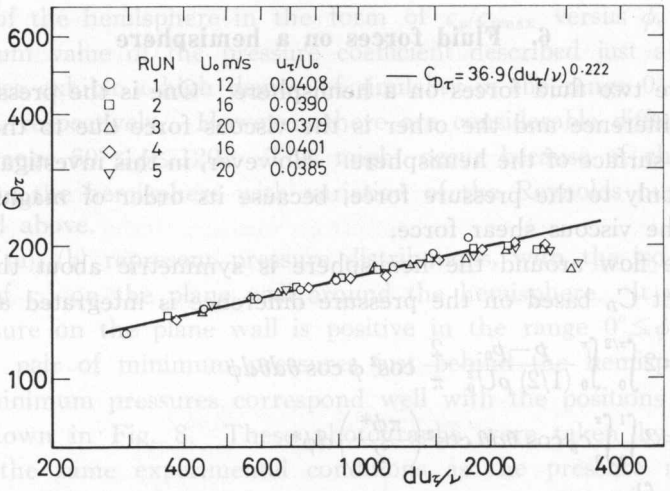

Fig. 10. Power function of $C_{D\tau}$ with respect to du_τ/δ.

repesenting the effect of u_τ/U_0 and fulfills the relationship of eqn. (4). The drag coefficient $C_{D\tau}$ is represented as derived from eqn. (5) in Fig. 10. It is clear that $C_{D\tau}$ is uniquely related to du_τ/ν in the range $d/\delta \leq 1.0$ and can be expressed by a power function :

$$C_{D\tau} = 36.9\,(du_\tau/\nu)^{0.222} \tag{12}$$

This result shows that the parameter u_τ/U_0 included in eqn. (6) has little influence on the drag coefficient $C_{D\tau}$ in this range.

The aerodynemic characteristics of three-dimensional bluff bodies such as right circular cylinders [7] and cubes [8] immersed in turbulent boundary layers were investigated earlier. It was found that the drag coefficient $C_{D\tau}$ could be expressed by power functions using the single parameter hu_τ/ν in the range $h/\delta \leq 1.0$, where h is the height of the bluff body. Those functional relationships are written as

$$C_{D\tau} = 39.2\,(hu_\tau/\nu)^{0.351} \tag{13}$$

$$C_{D\tau} = 44.8\,(hu_\tau/\nu)^{0.279} \tag{14}$$

in cases of cubes and right circular cylinders, respectively. Moreover, since d can be replaced by the height of the hemisphere $h(=d/2)$, expression (12) becomes

$$C_{D\tau} = 43.0\,(hu_\tau/\nu)^{0.222}. \tag{15}$$

When comparing eqns. (13)~(15), it will be seen that different values of the coefficient and power occur in these expressions. Although these differences might be considered to derive from the particular shape of each three-dimensional bluff body, a systematic dependence of the drag on the particular shape cannot be clarified yet. Nevertheless, it is interesting to note that the rate of increase of $C_{D\tau}$ with respect to hu_τ/ν becomes larger in order of cube, right circular cylinder and hemisphere, as represented by the magnitude of the powers included in eqn. (13)~(15). The reason for this trend of $C_{D\tau}$ might be considered to be

that the effectiveness of the blockage of the three-dimensional bluff body to the approaching flow is larger in order of the obstacles as listed above.

The variation of the lift coefficient C_L defined eqn. (7) is shown in Fig. 11. C_L is also plotted on a log-log sheet with respect to d/δ for the paremeter u_τ/U_0. As will be seen in this figure, C_L forms two groups of straight lines, which have nodal points in the region $0.75 \leq d/\delta \leq 1.0$ and are parallel with one another. However, C_{L_τ} expressed by eqn. (8) could not be plotted on a single line as C_{D_τ} shown in Fig. 9. Consequently, an experimental expression is induced from Fig. 11 as

$$C_D = b(d/\delta)^a, \tag{16}$$

where a is a constant number dependent on d/δ. It has the following values:

$$a = \begin{cases} 0.435 \ (d/\delta \leq 0.75 \sim 1.0) \\ 0.633 \ (d/\delta > 0.75 \sim 1.0) \end{cases} \tag{17}$$

The coefficient b is expressed as a function of u_τ/U_0 in the each region, as shown Fig. 12.

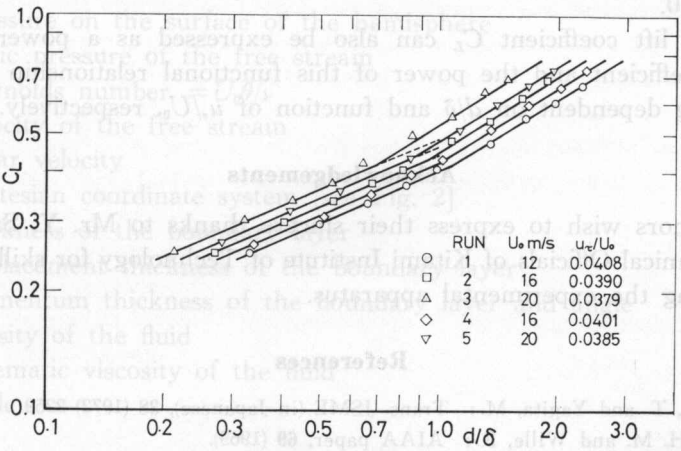

Fig. 11. Relation between the lift coefficient C_L and d/δ.

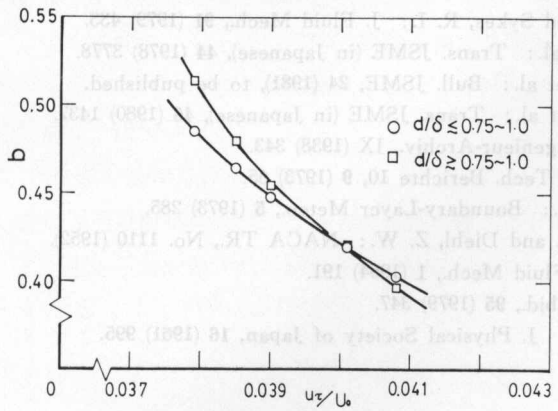

Fig. 12. Relation between coefficient b and u_τ/U_0.

7. Concluding remarks

Time-averaged pressure distributions on a hemisphere set up on a smooth plane wall on which a turbulent boundary layer was fully developed were measured in order to clarify the aerodynamic force experienced by the hemisphere. Measurements of the pressure were carried out, varying both the geometrical size of the hemisphere and the characteristics of the boundary layers. The main results obtained in the present investigation may be summarized as follows:

(1) The pressure distributions along the symmetric plane of the hemisphere are highly similar in the region $0° \leq \phi \leq 50°$ notwithstanding variations in both the size of the hemisphere and the characteristics of the boundary layer. However, the pressure distributions in the region $50° \leq \phi \leq 120°$ show a marked dependence on the Reynolds number.

(2) The drag coefficient defined by $C_{D_\tau} = D \Big/ \left(\frac{1}{2} \rho u_\tau^2 A \right)$ is uniquely related to du_τ/ν and can be expressed as a power function in the range $du_\tau/\nu \leq 2000$ when $d/\delta \leq 1.0$.

(3) The lift coefficient C_L can also be expressed as a power function of d/δ. The coefficient and the power of this functional relationship are constant number being dependent on d/δ and function of u_τ/U_0, respectively.

Acknowledgements

The authors wish to express their sincere thanks to Mr. Y. Saeki and Mr. K. Abe, Technical Officials of Kitami Institute of Technology for skillful assistance in constructing the experimental apparatus.

References

[1] Okamoto, T. and Yagita, M.: Trans. JSME (in Japanese), **38** (1972) 2259.
[2] Fiedler, H. M. and Wille, R.: AIAA paper, **69** (1969).
[3] Castro, I. P. and Robins, A. G.: J. Fluid Mech., **79** (1977) 307.
[4] Okamoto, T., et al.: Trans. JSME (in Japanese), **42** (1976) 2107.
[5] Mason, P. J. and Sykes, R. I.: J. Fluid Mech., **91** (1979) 433.
[6] Daiguji, H., et al.: Trans. JSME (in Japanese), **44** (1978) 3778.
[7] Taniguchi, S., et al.: Bull. JSME, 24 (1981), to be published.
[8] Sakamoto, H. et al.: Trans. JSME (in Japanese), **46** (1980) 1437.
[9] Jacobs, M.: Ingenieur-Archiv., IX (1938) 343.
[10] Wieghart, K.: Tech. Berichte 10, **9** (1973) 65.
[11] Wooding, R. A.: Boundary-Layer Meteo., **5** (1973) 285.
[12] Klebanoff, P. S. and Diehl, Z. W.: NACA TR., No. 1110 (1952).
[13] Coles, D.: J. Fluid Mech., **1** (1954) 191.
[14] Baker, C. J.: ibid., **95** (1979) 347.
[15] Mochizuki, M.: J. Physical Society of Japan, **16** (1961) 995.

Nomenclature

A: projectional area of the hemisphere $=\pi d^2/8$
a: power of the power function [see eqn. (16)]
b: coefficient of the power function [see eqn. (16)]
C_D: drag coefficient $=D/\left(\frac{1}{2}\rho U_0^2 A\right)$
C_{D_τ}: drag coefficient $=D/\left(\frac{1}{2}(\rho u_\tau^2 A\right)$
C_L: lift coefficient $=L/\left(\frac{1}{2}\rho U_0^2 A\right)$
C_{L_τ}: lift coefficient $=L/\left(\frac{1}{2}\rho u_\tau^2 A\right)$
D: drag force
H: shape factor $=\delta^*/\theta$
L: lift force
d: diameter of the hemisphere
p: pressure on the surface of the hemisphere
p_0: static pressure of the free stream
R_θ: Reynolds number $=U_0\theta/\nu$
U_0: velocity of the free stream
u_τ: shear velocity
x, y, z: Cartesian coordinate system [see Fig. 2]
δ: thickness of the boundary layer
δ^*: displacement thickness of the boundary layer
θ: momentum thickness of the boundary layer and angle
ρ: density of the fluid
ν: kinematic viscosity of the fluid
ϕ: angle